# X-ray Emissions from Comets Detected in the Röntgen X-ray Satellite All-Sky Survey

Konrad Dennerl,* Jakob Englhauser, Joachim Trümper

After the unexpected discovery of x-rays emitted from comet C/1996 B2 (Hyakutake) with the Röntgen X-ray Satellite (ROSAT) in March 1996, x-ray emissions from comets C/1990 K1 (Levy), C/1990 N1 (Tsuchiya-Kiuchi), 45P (Honda–Mrkos–Pajdušáková), and C/1991 A2 (Arai), optically 300 to 30,000 times fainter than Hyakutake, were discovered in archival ROSAT data. These findings establish comets as a class of x-ray sources and allow their properties to be studied over a wide optical brightness range. The results indicate that charge exchange between highly charged heavy ions in the solar wind and cometary neutrals is the dominant process for the x-ray emission. Comets may thus be used as probes for monitoring the heavy-ion content of the solar wind.

Comets have attracted attention since historical times. In this century, they have become subject to increasingly advanced astrophysical studies, which so far culminated in detailed observations of comet 1P/Halley, including in situ measurements, during its apparition in 1986. Nevertheless, one aspect of cometary activity seems to have escaped attention until recently, when unexpectedly strong x-ray emission was observed from comet C/1996 B2 (Hyakutake) with ROSAT (*1*). Although this discovery has demonstrated that a comet is capable of emitting x-rays, the mechanism and the conditions required to produce cometary x-rays were still uncertain. To get more information about cometary x-rays, we systematically searched archival x-ray data, which were obtained during the ROSAT all-sky survey in 1990 and 1991, for x-ray emissions from other comets. We investigated four comets, seen on seven occasions at different states.

Between July 1990 and February 1991, and in August 1991, ROSAT (*2*) performed the first survey of the whole sky with an imaging x-ray telescope. This ROSAT all-sky survey (RASS) (*3*) detected about 80,000 discrete sources (*4*) and obtained images of the diffuse x-ray emission at a resolution of 1 to 10 arc min (*5*). The survey was performed with a position-sensitive proportional counter (PSPC) (*6*) in the focal plane of a fourfold nested Wolter type I grazing incidence x-ray telescope (*7*), providing spatial, temporal, and spectral information on the detected x-ray photons in the energy range of 0.1 to 2.4 keV within a 2° field of view (FOV).

We searched the RASS database for x-ray signatures of comets that were within the PSPC FOV during the survey scans. For this search, we selected 214 comets (not counting multiple fragments) from the *Catalogue of Cometary Orbits* (*8*) with perihelion dates between 1985 and 1997. Eight comets were in the FOV when their heliocentric distances ($r_h$) were less than 2 astronomical units (AU), 17 comets were observed at $r_h$ between 2 and 3 AU, 164 comets were observed at $r_h > 3$ AU, and 25 comets were never observed. To obtain the maximum detection efficiency, we searched for x-ray emission in the rest frame of each comet. This was possible because the arrival time and the detector coordinates of each detected x-ray photon are recorded. Thus, we can track the apparent proper motion of the comet as seen from the satellite, given the satellite position and orientation together with the comet ephemeris (Fig. 1). By applying this method to all 25 comets observed at $r_h \leq 3$ AU, we discovered x-ray emission from four comets on seven occasions (*9*). We detected x-ray emission from all of the comets that were observed at $r_h \leq 2$ AU with total visual magnitude $m_1 \leq 12.0$ mag (Table 1). No emission was detected from comets at $r_h > 2$ AU or $m_1 > 12.0$ mag (*10*). Because comets at $m_1 \approx 12.0$ mag were close to the sensitivity limit, this is most likely a flux-limit effect.

An advantage of RASS compared with pointed ROSAT observations is that it provides an unlimited field of view and thus

**Table 1.** Comets in which x-rays were detected are listed. For comparison, we have added the corresponding parameters for x-ray detections of comets in recent pointed observations (*1, 13, 32*) obtained with the ROSAT High Resolution Imager (HRI) (*2*). obs. no. 1–7, ROSAT PSPC; obs. no. 8–10, ROSAT HRI. NO. indicates observation number. $t_{exp}$ is total exposure time (in seconds). The proper motion of the comets and the progression of the ROSAT survey scans resulted in different exposure times for different comets. $t_{obs}$ is time interval of observation (UT). This is the time interval during which the PSPC was scanning across a region within $r = 10'$ around the cometary nucleus (including partial scans); the outer regions of more extended comets were (partially) covered for somewhat larger time intervals. $\Delta$ is distance from Earth (in AU). $r_h$ is distance from the sun (in AU). Because of observing constraints, $r_h$ and $\Delta$ are not completely independent (*21*). $z_{ecl}$ is distance from the ecliptic plane (in AU). $\varphi$ is phase (angle sun–comet–Earth) in degrees. $\vartheta$ is elongation (angle sun–Earth–comet) in degrees. $m_1$ is total optical brightness (in mag). $r_c$ is radius of the optical coma (in arc min); $m_1$ and $r_c$, with estimated $1\sigma$ errors, were derived from data published in the *IAU Circulars* and the *International Comet Quarterly* (*39*). log $Q_{H_2O}$ is water production rate at $r_h$ (molecules $s^{-1}$). Values in brackets are estimates based on $m_1$, assuming that the dust-to-gas ratio of these comets was similar to the average value computed for the other comets (*40*). Abbreviations for comets are: T–K, Tsuchiya–Kiuchi; HMP, Honda–Mrkos–Pajdušáková; Hyak., Hyakutake.

| No. | Comet | $t_{exp}$ | | $t_{obs}$ | | $\Delta$ | $r_h$ | $z_{ecl}$ | $\varphi$ | $\vartheta$ | $m_1$ | $r_c$ | log $Q_{H_2O}$ |
|---|---|---|---|---|---|---|---|---|---|---|---|---|---|
| 1 | C/1990 K1 (Levy) | 77 | 1990 | Sep | 06.50–07.17 | 0.57 | 1.25 | −0.05 | 52 | 101 | 4.8 ± 0.4 | 6.0 ± 1.5 | 29.94 ± 0.01 |
| 2 | C/1990 K1 (Levy) | 269 | 1991 | Jan | 10.82 –11.96 | 1.39 | 1.62 | −0.72 | 37 | 84 | 7.5 ± 0.3 | 2.3 ± 1.0 | 29.04 ± 0.11 |
| 3 | C/1990 K1 (Levy) | 149 | 1991 | Jan | 17.49 –17.96 | 1.31 | 1.69 | −0.70 | 35 | 94 | 7.6 ± 0.4 | 2.6 ± 1.0 | 28.96 ± 0.11 |
| 4 | C/1990 N1 (T–K) | 460 | 1990 | Nov | 18.90 –20.36 | 1.08 | 1.37 | −0.66 | 46 | 83 | 7.8 ± 0.4 | 2.4 ± 0.8 | 28.69 ± 0.06 |
| 5 | C/1990 N1 (T–K) | 451 | 1991 | Jan | 12.07 –13.67 | 1.61 | 1.96 | −1.15 | 30 | 95 | 10.4 ± 0.7 | 1.1 ± 0.5 | 28.19 ± 0.16 |
| 6 | 45P (HMP) | 191 | 1990 | Jul | 31.20–31.86 | 0.29 | 1.00 | −0.06 | 86 | 78 | 11.8 ± 0.5 | 1.5 ± 0.5 | 26.89 ± 0.14 |
| 7 | C/1991 A2 (Arai) | 769 | 1990 | Nov | 18.09 –21.43 | 1.20 | 1.47 | −0.88 | 42 | 84 | 12.0 ± 0.5* | — | [27.29 ± 0.20] |
| 8 | C/1996 B2 (Hyak.) | 20,500 | 1996 | Mar | 26.52–28.43 | 0.12 | 0.99 | +0.10 | 91 | 82 | 0.8 ± 0.4 | 30. ± 12. | 28.90 ± 0.10 |
| 9 | C/1996 B2 (Hyak.) | 8900 | 1996 | Jun | 22.10–23.77 | 1.16 | 1.35 | −1.09 | 46 | 77 | 6.4 ± 0.5 | 3.3 ± 1.0 | 28.66 ± 0.12 |
| 10 | C/1996 Q1 (Tabur) | 11,500 | 1996 | Sep | 26.74–29.01 | 0.49 | 1.08 | +0.01 | 67 | 86 | 5.9 ± 0.5 | 6.0 ± 1.4 | [28.69 ± 0.20] |

*Projected value with estimated error, interpolated backward in time, because the comet was observed with ROSAT 6 weeks before it was discovered (*41*).

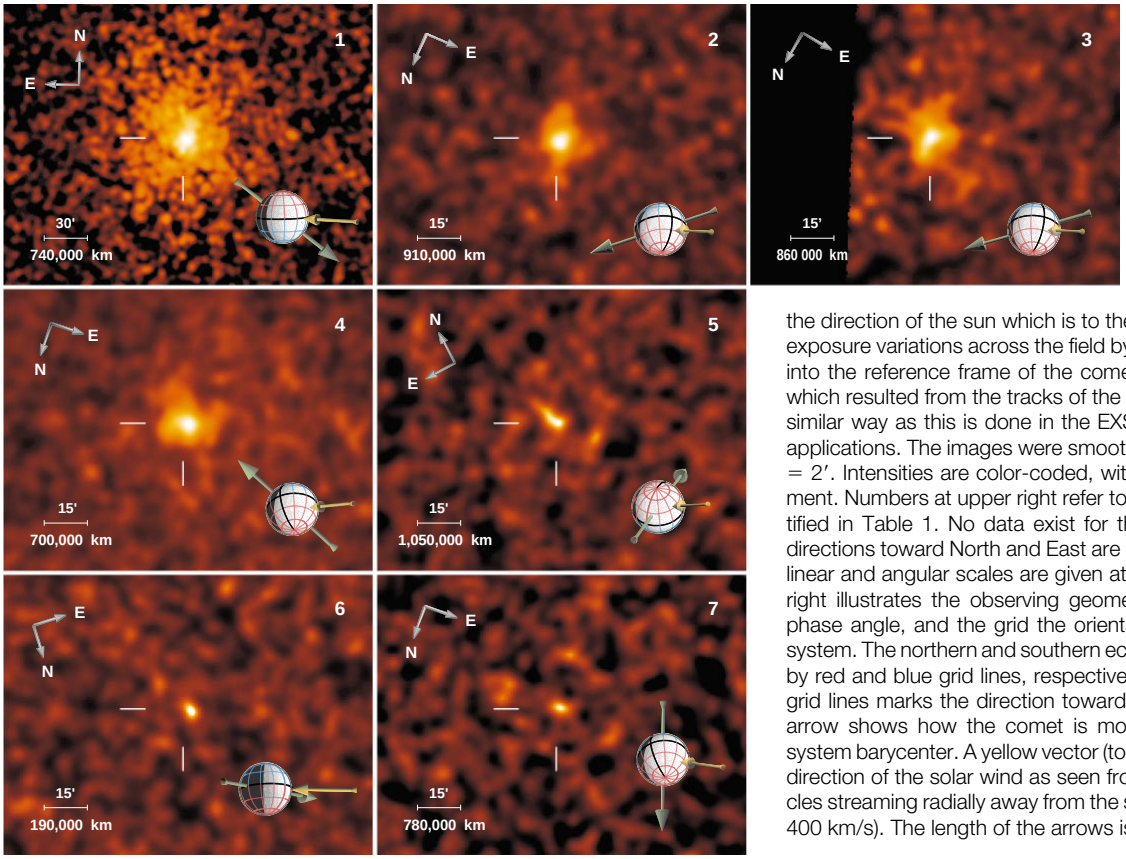


**Fig. 1.** X-ray images of the comets detected in the RASS in the energy range 0.1 to 0.4 keV, which contains more than 90% of the detected cometary photons. The images were accumulated in the rest frame of each comet (the position of the nucleus predicted by the ephemeris is marked) and aligned with respect to the direction of the sun which is to the right. They were corrected for exposure variations across the field by transforming the survey scans into the reference frame of the comet and simulating the exposure which resulted from the tracks of the detector across the image, in a similar way as this is done in the EXSAS package (*38*) for standard applications. The images were smoothed with a gaussian filter with $\sigma = 2'$. Intensities are color-coded, with an individual contrast adjustment. Numbers at upper right refer to the ROSAT observations identified in Table 1. No data exist for the left part of obs. no. 3. The directions toward North and East are marked in the upper left corner; linear and angular scales are given at lower left. The sphere at lower right illustrates the observing geometry: its illumination shows the phase angle, and the grid the orientation of the ecliptic coordinate system. The northern and southern ecliptic hemispheres are indicated by red and blue grid lines, respectively; the intersection of the black grid lines marks the direction toward the vernal equinox. The green arrow shows how the comet is moving with respect to the solar system barycenter. A yellow vector (touching the sphere) indicates the direction of the solar wind as seen from the moving comet (for particles streaming radially away from the sun with an assumed velocity of 400 km/s). The length of the arrows is arbitrary.

allows the full extent of the x-ray emitting region to be traced. Furthermore, the low instrumental background of the PSPC and its high sensitivity to low-energy (or "soft") x-rays makes it well suited for studying faint extended objects with soft spectra, thus balancing the low exposure times in the RASS. By following the surface brightness accumulated along radial rings around the brightest region, excluding the trails of background sources, we were able to trace the x-ray emission out to a radial distance of at least $2 \times 10^6$ km during the first observation of comet C/1990 K1 (Levy) (*11*, *12*).

During the second Levy observation (Fig. 2), the phase angle $\varphi$ (sun–comet–Earth angle) was only 37° and provided an almost complementary viewing geometry to the ROSAT observation of Hyakutake, which was observed at $\varphi \sim 90°$ [figure 2 of (*1*)]. At $\varphi = 37°$, the inner x-ray contour lines are less elongated than at $\varphi \sim 90°$, as expected for an x-ray luminous hemisphere around the comet nucleus which is about symmetric with respect to the sun–comet line. The outermost contour (Fig. 2) is elongated perpendicular to this line, and there are indications for a slight tilt of the axis of symmetry toward the direction of the solar wind as seen from the moving comet. This suggests that the x-rays were emitted from the sunward side of the coma. The observation took place when, at the position of the comet, its orbital plane was tilted by only 14.7° to our line of sight. Combined with the small $\varphi$, the viewing geometry was favorable for detecting any emission from the cometary plasma and dust tails, because of the amplification of the surface brightness along the line of sight. In fact, an antitail is evident on the optical image together with the regular tail. Nevertheless, none of the tails shows up in x-rays. Thus, there is no evidence that the x-ray emission is associated with either the plasma or dust tail.

A similar morphology is present in all the other observations, and there is no evidence for x-ray emission from the tail. Most of the x-ray images show emissions that are roughly spherically symmetric or elongated perpendicular to the sun–comet line, with the brightest peak usually offset sunward by some $10^4$ km, reminiscent of a bow-shock structure. Two exceptions to this morphology are C/1990 N1 in observation number (obs. no.) 5 and comet C/1996 Q1 (Tabur) (*13*), which showed jet-like structures. There is no clear dependence of the x-ray morphology on the velocity vector of the comet (Fig. 1).

For Hyakutake, only broadband photometry was available (*1*), but the comets in the RASS were observed with a proportional counter that provides an energy resolution of $\Delta E/E = 0.43 \cdot \sqrt{0.93/E}$ [keV] over a bandpass of 0.1 to 2.4 keV. Thus, spectroscopic studies of cometary x-ray emission are possible with unprecedented quality. In the seven observations, the emission is soft: about 95% of the detected photons are at $E < 0.4$ keV. This corresponds to 83% of the energy flux in the total PSPC bandpass. Although we can rule out certain spectral models—for example, a line spectrum consisting only of oxygen and carbon $K_\alpha$ fluorescence lines—the softness of the x-ray emission reduces the usable spectral bandwidth and does not allow determination of the incident spectrum in a unique way. For Levy, which had the largest number of recorded photons [186 within $r_x$ (*12*), including ≈11 background photons; obs. no. 1] we find acceptable fits for thermal bremsstrahlung ($kT = 0.23 \pm 0.06$ keV; Fig. 3) and emission from a hot ($kT = 0.12 \pm 0.02$ keV) optically thin plasma in thermal equilibrium [Raymond and Smith (*14*)] with solar abundance. Formally, a power law (photon index $\alpha = -3.0 \pm 0.3$) also fits the data, but the residuals indicate systematic deviations. Spectral analysis with a thermal bremsstrahlung model, which we have se-

The authors are at the Max-Planck-Institut für extraterrestrische Physik, Giessenbachstraße, D-85748 Garching, Germany.

*To whom correspondence should be addressed. E-mail: kod@mpe-garching.mpg.de

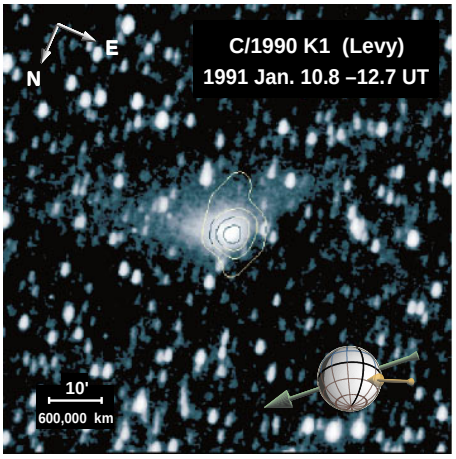


**Fig. 2.** Overlay of the x-ray contours of comet C/1990 K1 (Levy) on an optical image, taken nearly simultaneously with the ROSAT observations during 10.8 to 12.0 UT January 1991. The x-ray contours are drawn for 30%, 50%, 70%, and 90% of the peak surface flux; they were derived by smoothing the 0.1 to 0.4 keV ROSAT image with a gaussian filter with $\sigma = 2'$. The optical image is a 15-min exposure on hypered TP 2415 film, taken with a 200-mm F/4 lens on 12.7 UT January 1991 by P. Camilleri (Australia). The images have been aligned with respect to the direction of the sun, which is to the right. North and East are marked in the upper left corner; linear and angular scales are supplied at lower left. The sphere is described in Fig. 1. Note the presence of a secondary tail in the optical image toward the upper right.

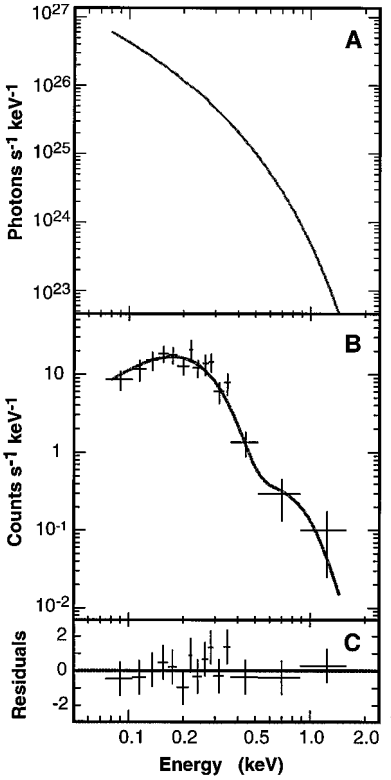


**Fig. 3.** X-ray spectrum of comet C/1990 K1 (Levy) during obs. no. 1. (**A**) Spectral model: photon spectrum of thermal bremsstrahlung emission with $kT = 0.23$ keV. (**B**) Crosses (with $1\sigma$ error bars): observed PSPC pulse height distribution in the energy range 0.08 to 1.4 keV. Solid line: pulse height distribution resulting from the model spectrum (A), after convolution with the ROSAT PSPC detector response matrix. (**C**) Residual deviations of the observed data (crosses with $1\sigma$ error bars) from the model, yielding $\chi^2 = 7.2$ for 13 degrees of freedom. The observed pulse height distribution is consistent with that expected from the model (A), with a probability of 89%.

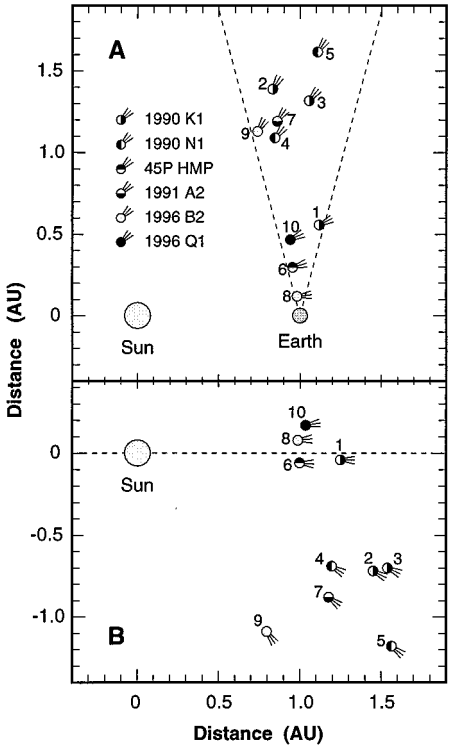


**Fig. 4.** Positions of the comets detected in x-rays with respect to (**A**) the sun and Earth and (**B**) the ecliptic plane [plane is indicated by dashed line in (B)]. The dashed lines in (A) enclose the ROSAT observing window. Different symbols indicate different comets, identified in (A). Numbers refer to the ROSAT observations listed in Tables 1 and 2.

lected because it provides a simple, straightforward method for estimating the characteristic temperature, shows that the temperatures of all comets are consistent with a mean value of $kT = 0.2$ keV (Table 2), independent of heliocentric distance, ecliptic latitude, or relative velocity between the comet and the solar wind (*15*).

Recently, Häberli *et al.* (*16*) made a detailed prediction of the energy spectrum that they expect to arise from the charge-exchange process suggested by Cravens (*17*). This spectrum is not compatible with the PSPC spectrum of comet Levy (*18*). The discrepancy, however, does not appear to be a general problem of the charge-exchange model, but mainly a consequence of an oversimplified treatment. In a more detailed analysis, Wegmann *et al.* (*19*) computed the x-ray spectrum that results from charge exchange of solar wind heavy ions with $H_2O$ molecules. This spectrum contains so many lines that, when observed with an instrument with moderate energy resolution, it resembles a $kT = 0.2$ keV thermal bremsstrahlung spectrum, in agreement with the observations. The seven comet detections in the RASS, together with the additional three detections in pointed observations (*1, 13, 20*), provide a database for studying cometary x-ray activity among different comets as well as among the same comets observed at different positions (*21*) in the inner solar system (Fig. 4).

To determine how the x-ray luminosity is related to the optical luminosity of the comets, we converted $m_1$ into an optical flux $f_{opt}$, by assuming a solar-like spectrum (*22*). This is a rough approximation that ignores the contribution of line emission in the gas coma. Nevertheless, because a considerable fraction of the optical flux comes from sunlight scattered in the dust coma, and in view of the uncertainties of $m_1$ and the fact that in our comparison $f_{opt}$ extends over more than four orders of magnitude, this approximation appears to be justified. We derived the x-ray flux $f_x$ in the energy range 0.1 to 2.4 keV within the HWHM radius $r_x$ (*12*), which, for similar x-ray surface flux distributions, encloses a constant fraction of the total $f_x$. To remove the effect of geocentric distance $\Delta$, we converted the fluxes $f$ into luminosities $L = f \cdot 4\pi\Delta^2$. We find that $L_x$ is about proportional to $L_{opt}$, although there are differences in the $L_x/L_{opt}$ ratio between different comets (Fig. 5). For Hyakutake, this ratio is only $(0.5 \pm 0.2) \times 10^{-5}$, whereas for the other comets, the average ratio is $(4.4 \pm 0.9) \times 10^{-5}$. There is no dependence of $L_x/L_{opt}$ on the phase in the solar activity cycle, on the heliocentric distance, on the distance from the ecliptic plane, or the relative velocity of the solar wind with respect to the comet. The differences may, however, be related to the ratio between the dust and gas in the coma. A measure for the dust production rate $Q_{dust}$ is the quantity $Af\rho$ (*23*); an empirical correlation was found (*24, 25*) that $Af\rho = 1$ cm roughly corresponds to a dust production rate $Q_{dust} = 1$ kg s$^{-1}$. A measure for the gas production rate $Q_{gas}$ is the production rate $Q_{H_2O}$ of water molecules per second. The quantity log ($Af\rho/Q_{H_2O}$) is –26.3 for 45P and C/1990 N1, –25.5 for C/1990 K1 (*25*), and –25.1 for C/1996 B2 (*26*). A comparison of the $L_x/L_{opt}$ and $Af\rho/Q_{H_2O}$ values (Fig. 5) suggests that $L_x$ is related to the gas content

**Table 2.** All x-ray fluxes and luminosities refer to an energy range 0.1 to 2.4 keV; uncertainties are estimated 1$\sigma$ errors. Values for obs. no. 8 through 10 are preliminary. The data analysis was based on EXSAS (*38*) algorithms adopted for moving targets. The x-ray luminosities may exhibit temporal variability: Hyakutake (*1*) and Tabur (*13*) were observed to be variable in x-rays on a time scale of hours. The RASS comet observations are averages of 5 to 18 individual scans of less than 32 seconds duration each, spread over 0.5 to 3.3 days (Table 1) and thus should provide representative samples of the average x-ray intensity. No., observation number. Comet, see Table 1 for full identification. $\tilde{s}_x$, observed peak surface flux ($10^{-12}$ erg cm$^{-2}$ s$^{-1}$ arc min$^{-2}$), determined by smoothing with a gaussian filter with $\sigma$ = 2′. $\hat{s}_x$, corrected peak surface flux ($10^{-12}$ erg cm$^{-2}$ s$^{-1}$ arc min$^{-2}$). $r_x$, angular HWHM radius (arc min), determined in the energy range 0.1 to 0.4 keV (*12*). $f_x$, flux within $r_x$ ($10^{-12}$ erg cm$^{-2}$ s$^{-1}$), determined for $kT$ = 0.2 keV. $L_x$, luminosity within $r_x$ ($10^{16}$ erg s$^{-1}$). $kT$, bremsstrahlung temperature (keV). $L_x/L_{opt}$, ratio of x-ray to optical luminosity in units of $10^{-5}$, for a solar-like comet spectrum.

| No. | Comet | $\tilde{s}_x$ | $\hat{s}_x$ | $r_x$ | $f_x$ | $L_x$ | $kT$ | $L_x/L_{opt}$ |
|---|---|---|---|---|---|---|---|---|
| 1 | Levy | 0.104 ± 0.035 | 0.066 ± 0.022 | 7.8 ± 0.4 | 12.7 ± 1.4 | 1.16 ± 0.12 | 0.23 ± 0.06 | 4.2 ± 1.6 |
| 2 | Levy | 0.022 ± 0.008 | 0.029 ± 0.011 | 4.3 ± 0.5 | 1.06 ± 0.23 | 0.58 ± 0.13 | 0.20 ± 0.10 | 4.2 ± 1.5 |
| 3 | Levy | 0.025 ± 0.011 | 0.035 ± 0.016 | 3.0 ± 0.9 | 0.71 ± 0.34 | 0.34 ± 0.17 | 0.60 ± 0.27 | 3.1 ± 1.9 |
| 4 | T-K | 0.022 ± 0.006 | 0.039 ± 0.011 | 3.6 ± 0.6 | 0.91 ± 0.24 | 0.30 ± 0.08 | 0.24 ± 0.12 | 4.8 ± 2.2 |
| 5 | T-K | 0.008 ± 0.003 | 0.047 ± 0.023 | 3.0 ± 0.9 | 0.24 ± 0.08 | 0.18 ± 0.06 | 0.28 ± 0.20 | 14. ± 11. |
| 6 | HMP | 0.006 ± 0.004 | 0.102 ± 0.073 | 1.9 ± 0.4 | 0.15 ± 0.06 | 0.004 ± 0.002 | 0.16 ± 0.15 | 31. ± 20. |
| 7 | Arai | 0.004 ± 0.002 | 0.100 ± 0.063 | 2.8 ± 0.3 | 0.08 ± 0.03 | 0.03 ± 0.01 | 0.34 ± 0.31 | 20. ± 12. |
| 8 | Hyak. | 0.300 ± 0.080 | 0.180 ± 0.048 | 7.2 ± 1.3 | 60.0 ± 20.0 | 0.24 ± 0.08 | [0.20] | 0.50 ± 0.24 |
| 9 | Hyak. | 0.053 ± 0.018 | 0.104 ± 0.040 | 1.7 ± 0.3 | 0.30 ± 0.12 | 0.11 ± 0.05 | [0.20] | 0.43 ± 0.27 |
| 10 | Tabur | 0.250 ± 0.090 | 0.279 ± 0.119 | 2.3 ± 0.2 | 7.00 ± 2.50 | 0.38 ± 0.14 | [0.20] | 7.0 ± 4.2 |

rather than the dust content in the coma, whereas $L_{opt}$ is known to be controlled mainly by cometary dust.

Another important photometric quantity is the peak surface flux $\hat{s}_x$, which is independent of $\Delta$. In the likely case that self-absorption of x-rays within the coma is negligible, it measures directly the maximum emission integrated along the line of sight. $\hat{s}_x$, however, is not necessarily identical to the observed peak surface flux $\tilde{s}_x$, derived from the ROSAT images (*27*). A correction from $\tilde{s}_x$ to $\hat{s}_x$ requires sufficient knowledge of the morphology and is not possible in a model-independent way. A promising model (see below) was suggested by Cravens (*17*) in which the x-ray emission results from charge transfer between highly charged heavy ions in the solar wind and cometary neutrals. With a simplified version of this model, we created a set of artificial images and treated them in the same way as the ROSAT images, to determine the $\tilde{s}_x/\hat{s}_x$ correction factors (Fig. 6A). In our model, we irradiated the neutral gas in the coma with a homogeneous beam of highly charged heavy ions, ignoring any hydrodynamic effects (*28, 29*). The use of such a simplified model for calibrating the $\tilde{s}_x/\hat{s}_x$ correction appears to be justified, because the resulting images reproduce the results of more detailed simulations (*16, 19*) and the observed morphology.

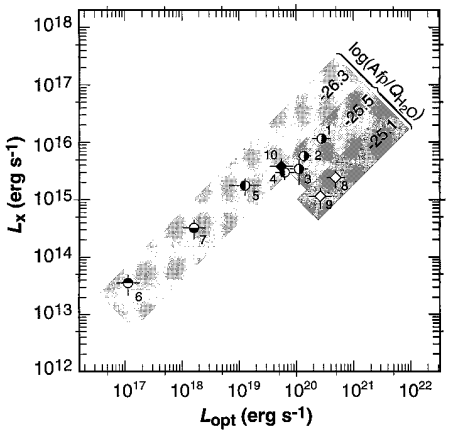


**Fig. 5.** Comparison between the optical and x-ray luminosity. Different symbols indicate different comets (identified in Fig. 4A). Numbers refer to the ROSAT observations listed in Table 1 and 2; circles and diamonds specify PSPC and HRI observations, respectively. Shaded regions illustrate the slope for constant $L_x/L_{opt}$ ratios, for different dust-to-gas ratios. The relative gas content increases from lower right to upper left.

The $\tilde{s}_x/\hat{s}_x$ calibration (Fig. 6A) shows that only for comets with log ($Q/\Delta$) $\gtrsim$ 29.5 is $\tilde{s}_x/\hat{s}_x$ independent of $Q/\Delta$: only these comets are "resolved" in the sense that $\hat{s}_x$ can be directly observed (*30*). If our simplified model is basically correct, then the calculated $\hat{s}_x$ should measure the highly charged heavy ion flux, for which we expect a general $r_h^{-2}$ dependence, corresponding to a temporally constant, isotropic solar wind (*31*). We do indeed find such a behavior (Fig. 6B). Furthermore, the $\hat{s}_x$ values are consistent with those predicted (*28*). Thus, the charge-transfer model (*17*) provides an adequate description of the observed peak surface fluxes.

Other models besides (*17*) have been proposed to explain the x-ray emission of comets. Wickramasinghe and Hoyle (*32*) suggested that the observed x-ray radiation may be due to scattering of solar x-rays by small (≈30 Å size) dust particles, which have a high scattering efficiency for soft x-rays. In view of the ROSAT observations, there are several problems. There is no significant difference in $\hat{s}_x$ or $L_x/L_{opt}$ between the comets observed in 1990 and 1991 during the solar maximum and the recent observations (*1, 13, 20*) at solar minimum. There is no evidence for x-ray emission from the dust tail, despite favorable observing geometries, and the presence of such dust at sufficient density in cometocentric distances $>10^6$ km has to be postulated in order to explain the large extent of the x-ray emission region.

Ip and Chow (*33*) suggested that small (diameter $\lesssim$ 100 Å) charged cometary dust grains may be accelerated by the electric field induced by solar wind interactions and collide with micrometer-sized grains in the dust coma, producing soft thermal x-rays. Estimates of the expected x-ray luminosity, however, show that this is unlikely to be the dominant process for generating the x-rays. Furthermore, the ROSAT observations (Fig. 5) indicate a correlation between $L_x/L_{opt}$ and $Q_{gas}/Q_{dust}$, which suggests that the x-ray emission is primarily related to the gas and not the dust content in the coma.

Several models have been suggested which invoke the acceleration of electrons in the solar wind or cometary cloud shocks (*34, 35*). The predicted x-ray luminosities, however, are highly uncertain [for example (*19, 35*)], and we were able to trace the x-ray emission to a cometocentric distance of at least $2 \times 10^6$ km. It is unlikely that the conditions prevailing at these distances are favorable for accelerating solar wind electrons to the required high velocities. This problem is also present if the x-ray emission is due to mini-flares in the cometary atmosphere, caused by the capture and squeezing of current sheets in the solar wind by the comet with subsequent magnetic reconnection and heating by magnetic-field annihilation (*36*). The fact that x-ray emission is observed as a persistent property of comets, related to their optical activity, is an argument

against any transient phenomena as the dominant processes, such as disconnection events or cometary substorms.

The suggestion that the x-ray emission is caused by charge exchange between highly charged heavy ions in the solar wind and cometary neutrals (*17*) avoids many of the difficulties of the other models. The existence of such ions is well established, and the gas coma provides the necessary amount of neutral atoms for charge exchange in a straightforward way. Even at $r_c > 10^6$ km, there should be sufficient matter for recombination, due to the huge extent of the hydrogen coma (Lyman-α cloud). The observation that only the sunward side of the coma is emitting x-rays, results from the fact that the inner coma is thick with respect to charge transfer, and the observed peak surface fluxes are in agreement with those expected. The nondetection of any cometary tail in x-rays is consistent with the fact that whenever a comet is sufficiently active to develop a plasma tail, its coma is so thick that the heavy ions have lost the highly charged state required to trigger x-ray emission by charge exchange processes before reaching the antisolar plasma tail. Heavy ions may reach part of the curved dust tail, which is not shielded by the coma, in a sufficiently charged state, but interactions with the cometary dust do not seem to release a significant amount of x-rays. This model predicts that x-ray luminosity should scale with the gas rather than the dust content in the coma, in agreement with the observations. There are several details which still have to be checked for this model: in particular, whether the predicted line spectra are in quantitative agreement with the observed pulse height distributions, whether the Lyman-α cloud can account for the x-ray brightness profile observed at large cometocentric distances, and whether fluctuations in the heavy-ion content of the solar wind can cause the time variability of the x-ray emission.

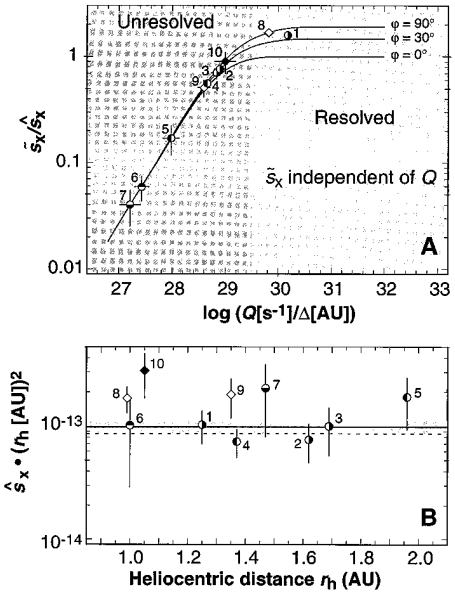


**Fig. 6.** (**A**) Ratio between the observed peak surface flux $\tilde{s}_x$ and the true peak surface flux $\hat{s}_x$ (normalized to $\hat{s}_x = 1.0$ for $\varphi = 0°$), resulting from smoothing a 30″ by 30″ pixel image with a gaussian filter with $\sigma = 2'$, for the model described in the text. In the "resolved" region, $\tilde{s}_x$ is independent of $Q$ and monitors the solar wind, whereas in the "unresolved" region, $\tilde{s}_x$ depends also on $Q$. The circles/diamonds (PSPC/HRI) and numbers mark the log ($Q/\Delta$) (with 1σ errors) and φ values for the comet observations; the vertical error bars indicate the resulting 1σ errors in the $\tilde{s}_x/\hat{s}_x$ correction. (**B**) Corrected peak surface flux $\hat{s}_x \cdot (r_h$ [AU])$^2$ (in erg cm$^{-2}$ s$^{-1}$ arc min$^{-2}$) for all comet detections as a function of $r_h$. The data are consistent with a mean value $1.0 \pm 0.1 \times 10^{-13}$ erg cm$^{-2}$ s$^{-1}$ arc min$^{-2}$ (shaded region) with a confidence of 31%. The dashed line, at $8.6 \times 10^{-14}$ erg cm$^{-2}$ s$^{-1}$ arc min$^{-2}$, is the value resulting from the parameters given in (*17*). It is only 1 standard deviation below the mean value.

The charge-exchange process would lead to interesting applications. As was demonstrated, the (corrected and normalized) $\hat{s}_x$ should scale directly with the highly charged heavy ion content in the solar wind. Thus, comets with a sufficiently dense coma could be used as "standard candles" for probing this specific property of the solar wind. With x-ray observations of high spatial resolution and sufficient signal-to-noise ratio, it might be possible to use comets for monitoring the temporal and spatial fluctuations of these solar wind ions in the inner solar system.

## REFERENCES AND NOTES


1. C. M. Lisse *et al.*, *Science* **274**, 205 (1996).
2. J. Trümper, *Adv. Space Res.* **2** (no. 4), 241 (1983).
3. W. Voges, in *Proceedings of Satellite Symposium 3: Space Sciences with Particular Emphasis on High-Energy Astrophysics*, from the "International Space Year" Conference, Munich, Germany, 30 March to 4 April 1992 (ESA ISY-3, 1992), p. 9.
4. W. Voges *et al.*, in preparation.
5. S. L. Snowden *et al.*, *Astrophys. J.* **454**, 643 (1995).
6. E. Pfeffermann *et al.*, *Proc. SPIE* **733**, 519 (1986).
7. B. Aschenbach, H. Bräuninger, G. Kettenring, *Adv. Space Res.* **2**, 251 (1983).
8. *Catalogue of Cometary Orbits* (Central Bureau for Astronomical Telegrams/Minor Planet Center, Smithsonian Astrophysical Observatory, Cambridge, MA, ed. 11, 1996).
9. K. Dennerl, J. Englhauser, J. Trümper, *IAU Circular 6404* (1996); *IAU Circular 6413* (1996); *IAU Circular 6472* (1996).
10. Comet 97P/1991 A1 (Metcalf-Brewington), which had $m_1 \approx 9$ mag at the time of its optical discovery on 7 January 1991 [H. J. Brewington, *IAU Circular 5155* (1991)], should have been of similar brightness during the ROSAT observations on 9.39 to 12.66 UT November 1990. The nondetection of this comet with ROSAT, despite a sufficient exposure of 770 s, would make this the only comet observed at $m_1 <$ 12 mag and $r_h < 2$ AU which was not detected in x-rays. A prediscovery photograph, however, showed that it was of $m_1 \approx 15$ mag only 41 hours before its discovery [M. Tanaka, *IAU Circular 5168* (1991)], indicating that the comet brightened rapidly just before it was discovered, probably due to an outburst. The ROSAT nondetection is therefore consistent with the brightness behavior of Metcalf-Brewington, which was probably at $m_1 > 12$ mag during the ROSAT observations. The only other comets which are known to have been observed during the RASS at $r_h \leq 2$ AU are 43P (Wolf-Harrington), 98P/1991 D1 (Takamizawa), and 124P/1991 F1 (Mrkos). At the time of the observation, they were as faint as 13.5, 16.0, and 18.0 mag, respectively. These comets are not detectable in the RASS, although a marginal signal from 43P may be present. In the obs. no. 1 through 4, the comets C/1990 K1 (Levy) and C/1990 N1 (Tsuchiya- Kiuchi) have also been detected in the 90- to 206-eV band with the Wide-Field Camera on ROSAT [J. P. Pye, R. G. West, K. Dennerl, *IAU Circular 6486* (1996)].
11. The emission may extend further out, but the x-ray surface brightness becomes so low that a detailed model of temporal variations of the PSPC background is essential for a determination of the full extent. During the survey, occasional increases in the overall soft x-ray background with a typical duration of up to 8 hours were detected. These "long-term enhancements" [M. Freyberg, thesis, Ludwig-Maximilians-Universitat, München, Germany (1994)] are a well-established, but unexplained phenomena. In view of the x-ray detections of comets, it is not unlikely that the solar wind interacts with the upper atmosphere of Earth in a similar way as it does with the coma of a comet, causing the sunward side of the geocorona to glow in x-rays. From the low ROSAT orbit, this glow would appear as a temporally variable soft component in the diffuse x-ray emission, as observed [M. Freyberg, K. Dennerl, J. Trümper, in preparation].
12. The variations of the soft x-ray background may cause systematic errors in the determination of the total x-ray flux from the comet. To minimize such errors, we used a circular aperture around the brightest area with a radius $r_x$ where the average surface flux $s_x$ has dropped to half of the observed peak surface flux $\tilde{s}_x$: $1/2\pi \cdot \int_0^{2\pi} s_x(r_x, \phi)\, d\phi = \tilde{s}_x/2$. With a maximum radius $r_x = 8'$ (Table 2), this aperture is so small that background inhomogeneities are negligible, while it is large enough to provide a useful signal to noise ratio: for a gaussian profile, it would contain exactly half of the emission. We used this aperture definition for the determination of the x-ray luminosities and for spectral studies.
13. K. Dennerl, J. Englhauser, J. Trümper, C. Lisse, *IAU Circular 6495* (1996).
14. J. C. Raymond and B. W. Smith, *Astrophys. J. Suppl. Ser.* **35**, 419 (1977).
15. The distribution of all seven *kT* values (Table 2) is consistent with the assumption of random scatter around a mean value, with a probability of 88.2% ($\chi^2 = 2.37$ for 6 degrees of freedom). The mean value is $\langle kT \rangle = 0.23 \pm 0.04$ keV.
16. R. M. Häberli, T. I. Gombosi, D. L. De Zeeuw, M. R. Combi, K. G. Powell, *Science* **276**, 939 (1997).
17. T. E. Cravens, *Geophys. Res. Lett.* 24.1, 105 (1997).
18. A fit of the predicted line spectrum [table 2 and figure 4 of (*16*)] to the PSPC spectrum of Levy, leaving the energies and relative intensities of the emission lines fixed and adjusting only the total intensity as a free parameter, yields $\chi^2 = 145$ for 14 degrees of freedom. The formal confidence of the fit is only $10^{-23}$.
19. R. Wegmann, H. U. Schmidt, C. M. Lisse, K. Dennerl, J. Englhauser, in preparation.
20. C. Lisse *et al.*, *IAU Circular 6433* (1996).
21. The fact that all of the observations were performed in the vicinity of Earth and at solar elongations (angle sun–Earth–comet, $\vartheta$) between 75° and 105°, imposes correlations between the distance of a comet from the sun ($r_h$) and Earth ($\Delta$) and its phase angle (sun–comet–Earth, $\varphi$): $r = \sqrt{1 + \Delta^2 - 2\Delta\cos\vartheta}$, and $2r\Delta\cos\varphi = \Delta^2 + r^2 - 1$.
22. E. Lamla, in *Landolt-Börnstein*, H. H. Voigt, Ed., Group VI, Vol. I, 5.2.6.0.3 (Springer Verlag, Berlin, 1965), p. 317.

23. $Af\rho$ is defined as the product of the dust albedo $A$, the filling factor $f$ of the dust within the aperture, and the projected radius $\rho$ of the aperture; it provides an aperture-independent measure of the dust production for a comet with a canonical spatial distribution of dust.
24. C. Arpigny *et al.*, *Atlas of Cometary Spectra* (Kluwer, Dordrecht, Netherlands, 1997).
25. M. F. A'Hearn, R. L. Millis, D. G. Schleicher, D. J. Osip, P. v. Birch, *Icarus* **118**, 223 (1995).
26. D. Schleicher *et al.*, *IAU Circular 6372* (1996).
27. Depending on the characteristic length of small-scale intensity variations, the distance $\Delta$ of the comet, the angular resolution of the instrument, and the photon statistics, $\hat{s}_x$ may be an average over more extended regions and thus different from $\hat{s}_x$. As a compromise between high spatial resolution and sufficient signal to noise ratio, we determined $\bar{s}_x$ by binning the photons into 30″ by 30″ pixels and smoothing the images with a gaussian filter with $\sigma$ = 2′.
28. According to Cravens (*17*), we used the following parameters: cross section, $\sigma = 3.0 \times 10^{-15}$ cm$^2$; expansion velocity in the coma, $v_c = 1.0$ km s$^{-1}$; velocity of the solar wind, $v_{sw} = 400$ km s$^{-1}$; density of solar wind ions, $n_{sw} = 10$ cm$^{-3}$; fraction of heavy ions, $f_h = 0.001$; x-ray yield, $f_y = 0.1$; energy released per heavy ion, $E_{ion} = 0.2$ keV. The neutral gas density profile in the coma was assumed to be $n_c(r_c) = Q_a/4\pi v_c r_c^2$where $r_c$ is the cometocentric distance and $Q_a = 1.5 \cdot Q_{H_2O}$. The gas production rate $Q_{H_2O} = 2 \times 10^{29}$ s$^{-1}$ adopted by Cravens for obs. no. 8 referred to a measurement on March 24.5 UT, when $Q$ was systematically higher than during the ROSAT observations from March 26.5 to 28.4 (*26*).
29. This simplified model has several interesting implications: (i) The volume emissivity scales directly with the heavy ion flux, and so does the integrated column density. Thus, a change in the heavy ion flux (that is, in $v_{sw}$, $n_{sw}$, or $f_h$) causes each image pixel to change in intensity by the same factor, leaving the HWHM radius $r_x$ unaffected. Uncertainties in $f_y$ or $E_{ion}$ have similar consequences. There is, however, a limitation in this simplified model: for high gas production rates, $r_x$ becomes so large that the assumption of a $n_c(r_c) \sim r_c^{-2}$ density profile is no longer valid. Formally, a gas production rate $Q = 10^{29}$ s$^{-1}$ would yield $r_x = 1.8 \times 10^5$ km. For $Q/\Delta$ below $10^{28}$ s$^{-1}$ AU$^{-1}$, $r_x$ becomes smaller than 1′ and thus difficult to resolve. (ii) A change in the gas production rate $Q$ causes each dimension of the image to scale in size by the same amount, leaving the peak surface flux unaffected. Uncertainties in the cross section $\sigma$ or the coma expansion velocity $v_c$ have the same effect. This is a consequence of the $n_c \sim r_c^{-2}$ density profile in the coma: for $\bar{n}_c = f \cdot n_c$, $\bar{r}_c = f \cdot r_c$, $\bar{z} = f \cdot z$, it follows that $\bar{n}_c(\bar{r}_c)\, d\bar{z} = n_c(r_c)\, dz$. Thus, the angular size of a comet in x-rays is mainly determined by the ratio $Q/\Delta$. (iii) The coma is thin (transparent) for x-rays but in its inner part usually thick with respect to charge transfer: $\hat{s}_x$ is independent of $Q$ down to $Q_{min} = 2.8 \times 10^{25}$ s$^{-1}$. $R_n$, for a nucleus with radius $R_n$ (in km). Thus, for $Q > Q_{min}$ [that is, for all comets in our sample (Table 1)], $\hat{s}_x$ is limited by the energy supply of the highly charged heavy ions in the solar wind; it scales with the product of the density and velocity of these ions, which should exhibit an $r_h^{-2}$ dependence on average. (iv) The peak surface flux at $\varphi = 0°$ and $r_h = 1$ AU is: $\hat{s}_x = v_{sw} n_{sw} f_h f_y E_{ion} = 1.3 \times 10^{-5}$ erg cm$^{-2}$ s$^{-1}$ = $8.6 \times 10^{-14}$ erg cm$^{-2}$ s$^{-1}$ arc min$^{-2}$. (v) Because the emission volume is not spherically symmetric and self-absorption of x-rays in the coma is negligible, $\hat{s}_x$ increases with $\varphi$, reaching a maximum at $\varphi = 90°$ which exceeds $\hat{s}_x$ at $\varphi = 0°$ by a factor of about 2. We define $\hat{s}_x$ as the peak surface flux observed at $\varphi = 0°$.
30. We note that "resolved" in this context is different from the usual definition, which compares the observed brightness distribution with the point spread function of the imaging device.
31. The $\bar{s}_x/\hat{s}_x$ correction does not depend on the solar wind parameters $n_{sw}$, $v_{sw}$, $f_h$ or on $f_y$ or $E_{ion}$. The only parameters that affect the correction curves (Fig. 6A) are the expansion velocity $v_c(r_c)$ [and thus the density profile $n_c(r_c)$] and the cross section $\sigma$. The fact that in all cases the correction leads to a comparable $\hat{s}_x$ (when normalized to the same $r_h$) indicates that the assumed values of $v_c(r_c)$ and $\sigma$ are not unreasonable (*37*). Because the peak surface fluxes are also close to the value expected for the chosen solar wind parameters, all assumptions are self-consistent.
32. N. C. Wickramasinghe and F. Hoyle, *Astrophys. Space Sci.* **239**, 121 (1996).
33. W. H. Ip and V. Chow, *Icarus*, in press.
34. R. Bingham, J. M. Dawson, V. D. Shapiro, D. A. Mendis, B. J. Kellet, *Science* **275**, 49 (1997).
35. T. G. Northrop, C. M. Lisse, M. J. Mumma, M. D. Desch, *Icarus* **127**, 246 (1997).
36. J. Brandt, C. Lisse, Y. Yi, *Bull. Am. Astron. Soc.* **189**, 25.05 (1996).
37. The coma expansion velocity $v_c$ depends on the heliocentric distance $r_h$. The dependence, however, is too weak to alter the $\bar{s}_x/\hat{s}x$ correction significantly: from $r_h = 1$ AU to $r_h = 2$ AU (the range of our sample), $v_c$ decreases by less than 10% [for example, H. L. F. Houpis and D. A. Mendis, *Moon Planets* **25**, 95 (1995)].
38. H. U. Zimmermann *et al.*, *EXSAS User's Guide*, MPE Report 257 (ROSAT Scientific Data Center, Garching, Germany, ed. 4, October, 1994).
39. *The International Comet Quarterly*, D. Green, C. Morris, S. Nakano, Eds. (Smithsonian Astrophysical Observatory, Cambridge, MA, 1989–91), vols. 11–13.
40. For the obs. no. 1 through 6, the gas production rates were determined from log $Q_{H_2O(q)}$, the water production rates at perihelion, and the dependence of $Q_{OH}$ on $r_h$ (*25*) (for obs. no. 6, the average slope –2.7 was used). For obs. no. 8, $Q_{r_h}$ was taken from (*24*), assuming $Q_{H_2O} \approx Q_{OH}$. This value was extrapolated to obs. no. 9 with the average −2.7 slope and compared with the log ($Q_{r_h}/\Delta$) determined from the $m_1$ values of C/1996 B2 (see below); the weighted average of both values was taken. For the obs. no. 7 and 10, $Q_{r_h}$ had to be determined from $m_1$, as no other information was available. This was done by assuming that the optical flux scales with $Q\ \Delta^{-2}\ r_h^{-2}$: the average value log $Q + 0.4 \cdot m_1 - 2$ log $\Delta -$ 2 log $r_h$ was calculated from obs. no. 1 through 6 and 8, and used for the estimate log $Q \approx 31.6 - 0.4\, m_1 + 2$ log $\Delta + 2$ log $r_h$.
41. H. Kosai, *IAU Circular 5157* (1991).


42. We thank C. Lisse, B. Aschenbach, F. Favata, M. Freyberg, W.-H. Ip, K. Jockers, E. Rieger, H.-U. Schmidt, S. Snowden, R. Treumann, and R. Wegmann for interesting and stimulating discussions. We are grateful to P. Camilleri for supplying the optical image of comet C/1990 K1. The ROSAT project is supported by the German Bundesministerium für Bildung, Wissenschaft, Forschung und Technologie (BMBF/DARA) and the Max-Planck-Gesellschaft.


# STATs and Gene Regulation


James E. Darnell Jr.



STATs (signal transducers and activators of transcription) are a family of latent cytoplasmic proteins that are activated to participate in gene control when cells encounter various extracellular polypeptides. Biochemical and molecular genetic explorations have defined a single tyrosine phosphorylation site and, in a dimeric partner molecule, an Src homology 2 (SH2) phosphotyrosine-binding domain, a DNA interaction domain, and a number of protein-protein interaction domains (with receptors, other transcription factors, the transcription machinery, and perhaps a tyrosine phosphatase). Mouse genetics experiments have defined crucial roles for each known mammalian STAT. The discovery of a STAT in *Drosophila*, and most recently in *Dictyostelium discoideum*, implies an ancient evolutionary origin for this dual-function set of proteins.


A large number of extracellular signaling polypeptides (>35) interact with specific cell surface receptors that trigger the activation of latent cytoplasmic transcription factors termed STATs. The STATs become phosphorylated on tyrosine, then dimerize by reciprocal SH2 phosphotyrosine interaction and enter the nucleus to regulate transcription of many different genes. The STATs were recognized as ligand-induced transcription factors in interferon (IFN)-treated cells and then in cells and tissues exposed to many other signaling polypeptides (*1–3*). A great deal of new information has accumulated about specificity in the activation of the STATs, about the functional domains of the proteins, and about the variety of their biologic functions both in development and in adults. Also, knowledge is beginning to accumulate about how STATs effect transcriptional changes.


The author is in the Laboratory of Molecular Cell Biology, Rockefeller University, New York, NY 10021, USA.


## Mechanism of Activation

Seven mammalian STAT genes have been identified in three chromosomal clusters (*4*). The genes encoding Stats 1 and 4 map to a region of mouse chromosome 1 (equivalent to human chromosome 2, bands q12 to q33); Stats 3, 5A, and 5B map to a region of mouse chromosome 11 (human chromosome 12, bands q13 to q14-1); and Stats 2 and 6 map to a region of mouse chromosome 10 (human chromosome 17, bands q11-1 to q22). Stats 1, 3, 4, 5A, and 5B are between 750 and 795 amino acids long, whereas Stats 2 and 6 are ~850 amino acids long (*2, 5* ) (Fig. 1). Differential splicing leads to the production of a number of additional proteins, but the extent of variable splicing has not been widely explored. An important unresolved issue is whether